Journal of Materials Chemistry B

Co-caged Gold-Nanoclusters and Methyl-Motifs Lead to Detoxification of Dendrimers and Allow Cytosolic Access for siRNA Transfection

Journal:	*Journal of Materials Chemistry B*
Manuscript ID:	TB-ART-07-2014-001153.R1
Article Type:	Paper
Date Submitted by the Author:	30-Jul-2014
Complete List of Authors:	Chien, Chih-Te; National Health Research Institutes, Liu, Chia-Yeh; National Health Research Institutes, Wu, Zong-Wei; National Health Research Institutes, Chen, Pin-Jyun; National Health Research Institutes, Chu, Ching-Liang; Graduate Institute of Immunology, Lin, Shu-Yi; National Health Research Institutes, Institute of Biomedical Engineering and Nanomedicine

Cite this: DOI: 10.1039/c0xx00000x

www.rsc.org/xxxxxx

ARTICLE TYPE

Co-caged Gold-Nanoclusters and Methyl-Motifs Lead to Detoxification of Dendrimers and Allow Cytosolic Access for siRNA Transfection

Chih-Te Chien,[a] Chia-Yeh Liu,[a] Zong-Wei Wu,[a] Pin-Jyun Chen,[a] Ching-Liang Chu*[b] and Shu-Yi Lin*[a]

Received (in XXX, XXX) Xth XXXXXXXXX 20XX, Accepted Xth XXXXXXXXX 20XX
DOI: 10.1039/b000000x

Nonviral vectors, such as cationic polymers and dendrimers, in gene delivery have encountered two major barriers in the form of inherent toxicity and inefficient cytosolic access that must be overcome. In this work, a simple co-caging strategy focused on overcoming the two limitations of dendrimers for siRNA transfection is reported. By embedding gold nanoclusters, the structure of dendrimer becomes compact to allow an irreversible backfolding of exterior primary amines from the branch to the core, which dramatically eliminates the dendrimer toxicity for safety. Again, gold nanoclusters with strong emissions can render the dendrimers with a trackable function as a transfection vector (denoted as TV) for siRNA transfection. In order to maximize complex efficiency with siRNA, the TV further caged methyl-motifs, transforming the partially tertiary amines to quaternary ammonium ions to form methylated TV (denoted as MTV). The cellular responses to the MTV were similar to those of the TV, but the responses to the MTV can also enhance cytosolic access to better deliver siRNA for mRNA knockdown. This finding provides a novel perspective to facilitate various cationic polymers for detoxification in biological applications through a co-caging strategy without further chemical modifications.

Introduction

Nonviral vectors, such as cationic polymers, designed for achieving RNAi-based therapeutics have been established to overcome the delivery challenge of making nuclease-susceptible siRNA molecules enter cells to interrupt the activity of specific genes, further down-regulating their protein expressions.[1-6] Such the potential applications, however, have encountered two major barriers in the form of inherent toxicity and inefficient cytosolic access that must be overcome. Compared to other cationic polymers, the amine-terminated polyamidoamine (PAMAM) dendrimers (G_nNH_2) are known to have highly dense charges that efficiently protect and deliver siRNA for the following transfection.[1] Through the difference of amine basicity between core and branch, the tertiary (core) and primary (branch) amines of PAMAM dendrimers can be protonated under physiological and endosomal conditions, respectively, to perform their own functions. At physiological pH (7.4), only the primary amines (1^o-amines) of dendrimers can be protonated to either interact or assemble spontaneously with the cell membrane, forcing intracellular uptake.[7] After attaching to the endosomal pH, the interior tertiary amines (3^o-amines) of PAMAM can be initiated as sponges to attract protons, increasing water influx into the endosome to induce endosomal swelling, which results in turn in endosomal breakdown.[8, 9] Unfortunately, unmodified cationic PAMAM dendrimers as delivery vectors can also damage cell membranes through the 1^o-amines, possibly forming irreversible pores of lipid bilayers associated with cell death.[7, 10-13] As a result, advanced strategies based on the 1^o-amine decoration of PAMAM dendrimers have been developed to overcome its intrinsic cytotoxicity.[14-21] However, the decorations of PAMAM dendrimers can often affect renal excretion ($\leq$ 5.5 nm)[22-25] because of the increase in hydrodynamic size or the inversion of their surface charges, finally resulting in a higher accumulation in the liver, kidney, and other organs compared to unmodified PAMAM dendrimers.[22, 24] Additionally, the efficiency of cytosolic delivery may be affected by the surface modification,[26] because the cavity polarity of amine-terminated PAMAM dendrimers can be inversed from hydrophilic to hydrophobic, which would inhibit water efflux and the "proton sponge" effect.[26, 27]

Here, we report a simple strategy (Fig. 1A) based on co-caging gold-nanoclusters and methyl-motifs within a fourth-generation amine-terminated PAMAM dendrimer (i.e., G_4NH_2), which can lead to the detoxification and cytosolic access of dendrimers. We found that the size of the G_4NH_2 caging gold-nanoclusters was smaller than that of the parent G_4NH_2. The "featured size contraction" can be attributed to a specific interaction between the dendrimer backbone and gold-nanocluster. Specifically, the size contraction forces the dendrimer structure to become compact and allow an irreversible backfolding of the exterior amines (i.e., 1^o-amines) to contact with the gold surface within the dendrimer cavity, which dramatically reduces the toxicity of the dendrimers, enhancing their safety. Furthermore, the gold nanoclusters with strong emissions at 460 nm, is predominately

emitted from an Au_8-cluster (a gold nanocluster with eight atoms, denoted as Au_8). This unique photoluminescence endows the dendrimers with a trackable function as a transfection vector (hereafter denoted as TV) for siRNA transfection. For maximizing complex efficiency with siRNA, the TV further caged methyl-motifs, transforming the partially tertiary amines (3^o-amines) to quaternary ammonium ions (4^o-ammonium ions) to form methylated TV (hereafter denoted as MTV). The cell response to the MTV was also similar to those of the TV but can also enhance cytosolic delivery, allowing the delivery of siRNA for mRNA knockdown. Using this co-caging process to derive the MTV, we demonstrated the detoxification and cytosolic access of dendrimers for siRNA transfection (Fig. 1B).

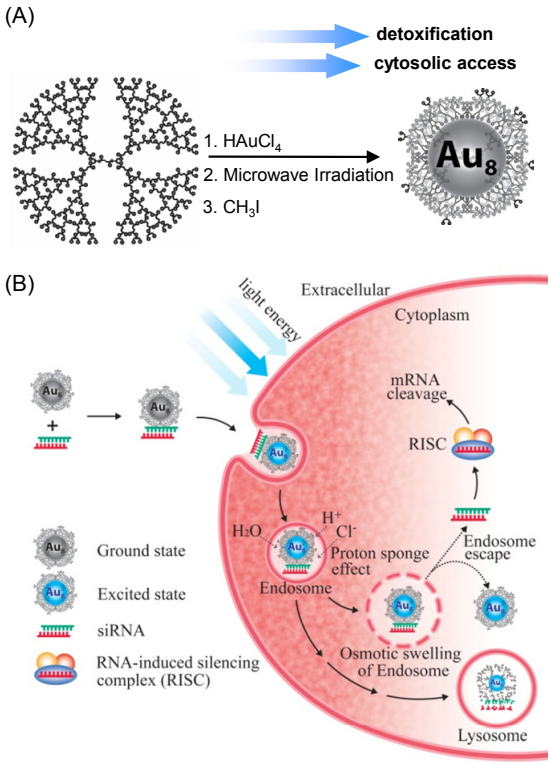

Fig. 1 Schematic representation of (A) a co-caging strategy for the dendrimer detoxification and cytosolic access, (B) the MTV as a trackable vector for siRNA transfection, in which the MTV/siRNA complex was taken up into cells by endocytosis and needed to escape from the endosome into the cytoplasm for mRNA targeting.

Experimental section

Materials

The G_4NH_2 dendrimer (Mw~14214 Da, each G_4NH_2 with 64 amine end groups), and methyl iodide were purchased from Sigma-Aldrich, and a 0.22-μm membrane filter was received from Millipore (PES membrane). The sequence of siRNA targeted to Bcl-2 mRNA: 5'-CCG GGA GAU AGU GAU GAA GdTdT-3' (sense strand)/5'-CUU CAU CAC UAU CUC CCG GdTdT-3' (antisense strand) and nonspecific siRNA used as a negative control: 5'-UGG UUU ACA UGU CGA CUA AdTdT-3' (sense strand)/5'-UUA GUC GAC AUG UAA ACC AdTdT-3' (antisense strand) were customized by BioNeer. Antibodies were purchased from Calbiochem (mouse anti-GAPDH), and Millipore (mouse anti Bcl-2 and goat anti mouse ITV conjugated HRP). PVDF membranes and ECL plus Western Blotting Detection Reagents (RPN2132) were purchased from GE Healthcare. All other materials were obtained in analytical quality.

Synthesis of TV and MTV

The gold-nanocluster was synthesized according to a previously published method.[28] First, $HAuCl_4$ (Sigma-Aldrich, 200 μL, 30 μmol, 150 mM) was added into 20 mL of deionized water containing the G_4NH_2 (Aldrich, 94.9 μL, 5 μmol, 20 wt % methanol solution). The G_4NH_2 and $HAuCl_4$ mixed solution was incubated at 4^oC overnight before irradiating by microwave (CEM, Discover LabMate System, 300W/120^{o}C for 30 min). The precipitations and gold nanodots after reduction were filtered through a 3 KDa MWCO membrane filter (Millipore, Amicon Ultra), and the extra anion ($AuCl_4^-$) was removed by using anionic exchange chromatography (Merck, Fractogel® EMD TMAE Hicap) to obtain the purified TV. Then, the internal tertiary amine groups and the surface amine groups of dendrimer encapsulated gold nanodots (63.6 mg, 4 μmol) were treated with methyl iodide in N,N'-dimethylformamide/H_2O (1 mL/1 mL) at room temperature overnight. The reaction mixture was extracted by dichloromethane 3 times and then dried under a vacuum and dissolved in water (1 mL). The resulting solution was then lyophilized to derive a white solid (i.e., MTV).

Cytotoxicity assay

The experiments of cell culture were performed in culture medium with 10% fetal bovine serum (FBS). The cells were inoculated into a 24-well cell-culture plate (1×10^5 cells/well) and cultivated for 24 h at 37^oC. Then, the culture medium was changed by the presence of various treatment concentrations, including G_4NH_2 alone, TV, and MTV, in culture mediums (three replicates). The tests were performed for 24 h without changing the medium. After removing the supernatant from the cell-culture medium, the cells were incubated with WST-1 (Clontech) at 37°C for 1 h. After treatment, the mediums were quantified using a conventional ELISA reader at 450 nm. For calibration, a blank test was performed on the same 24-well plate under the same condition.

Generation of mouse bone-marrow-derived DCs

DCs were generated from mouse bone marrow as described previously.[29] Briefly, bone marrow cells were isolated from the femurs and tibia of C3H mice. After removing red blood cells, the cells (1×10^6/well) were then seeded in 24-well culture plates with RPMI 1640 medium (Gibco) supplemented with 10% heat-inactivated FBS, 2 mM l-glutamine, nonessential amino acids, sodium pyruvate, HEPES (all from Invitrogen Life Technologies), 2-ME (Sigma-Aldrich), 100 U/mL penicillin, 100 μg/mL streptomycin and 10 ng/mL recombinant mouse GM-CSF (PeproTech). On day 6 or 7, the DCs (> 70%) were collected for analysis.

Assay for TNF-α production by DCs and DC maturation

As previously described,[30] TNF-α production by DCs was determined using intracellular cytokine staining. DCs were treated with LPS, TV, and MTV for 6 h and with the protein transport inhibitor GolgiPlug (BD Pharmingen) for 4 h. Cells were washed and stained with anti-CD11c and anti-TNF-α Ab

using the Fix and Perm Cell Permeabilization Kit (BioLegend). The production of TNF-α by DCs was measured by flow cytometry gating on CD11c+ cells. For the maturation assay, DCs were treated with LPS, TV, and MTV for 24 h and then stained with Abs specifically for MHC class II, CD11c, and CD86 (eBioscience). The expression levels of MHC-II and CD86 of DCs were analyzed by flow cytometry gating on CD11c+ cells.

Quantification of the residual amines on TV and MTV using ninhydrin-based assay

Sodium acetate (3.28 g) was dissolved in approximately 6 mL of DI water as a buffer. The pH of the resulting solution prepared by sodium acetate (3.28 g) in 6 mL DI was adjusted to 5.2 using glacial acetic acid, and the final volume was diluted to 10 mL. The ninhydrin reagent was freshly prepared by adding 4M sodium acetate buffer (1 mL to 80 mg ninhydrin and 12 mg hydrindantin in 3 mL DMSO). For the assay, 50 μL of reagent was added to 50 μl of the sample (2.8 nmol for G_4NH_2) in a tube. The tube was mixed for 15 s and incubated at 37°C for 3 h to allow the reaction to proceed. After incubation, 1900 μL of a 50:50 mixture of ethanol and water was added to each tube. The resulting solution was then mixed for 15 s to oxidize the excess of hydrindantin. The absorbance of each solution was measured on a UV spectrophotometer at approximately 560 nm, and the concentration of 1°-amine in the sample was calculated from a standard calibration curve.

Measurement of the sizes of TV and MTV using polyacrylamide gel electrophoresis (PAGE)

Various PAMAM dendrimers were loaded on a vertical electrophoresis system (Mini Trans-Blot®cell, BIO-RAD, USA) with a commercial power supply (MP-250V, Major Science). Precast 4-20% gradient express gels for PAGE were purchased from BIO-RAD (Mini-PROTEAN® TGX™ Gels; each gel has 10-well combs, 30μL/well). The citrate buffer (pH 3.0, 500 mL) was prepared as a running buffer. PAGE separation typically required 180 min at 60 V. An aliquot (10 μL) of the sample solution composed of 8.4 μg PAMAM dendrimer (5 mg/mL, 1.67 μL) and 1.67 μL sucrose solution (50% sucrose) was injected into each well. Developed gels were stained with 0.025% coomassie brilliant blue R-250 in 40% methanol and 7% acetic acid aqueous solution for 30 min. The gels were destained with 7% v/v acetic acid and 5% v/v methanol in water.

Gel electrophoresis

The binding capacity was expressed by the N/P ratio, which was defined as the number of nitrogen residues (N) in the surface of dendrimer per phosphate (P) of siRNA. It showed a total retardation of siRNA migration (as reflected by the disappearance of siRNA bands on the gel). The complexes of different modified dendrimers and siRNA were prepared in water containing either FBS or not, at various N/P ratios and incubated at room temperature for 30 min, followed by incubation with RNase for 15 min. Dendrimer-free siRNA was used as the control. The samples were further diluted with PBS buffer and electrophoresed in 2% agarose gel at 100 V for 30 min in Tris-boric acid (TBE) running buffer, then staining with ethidium bromide (EB). siRNA bands on the gel were visualized under ultraviolet light (254 nm).

Western blot after nanoplexes delivery

The silence efficient assay was performed under culture medium supplemented 10% FBS. To assess the silencing capability of various nanoplexes, HEK293 cells were plated in 6-well plates at a seeding density of 1×10^5 cells per well. The cells were left overnight to adhere. The next day, the cells were transfected with various formulations at a final siRNA dose (3.3 μg/mL) as the following treatments for 48 h: the mixture of siRNA and Lipofectamine as a positive control, naked siRNA, and siRNA loaded different modified dendrimer nanoparticles (i.e., TV and MTV) under the N/P ratio of 25:1. Untreated cells were used as the negative control. Following treatment, the total protein was extracted and the protein content was measured using the BCA Protein Assay Kit (Thermo). The extracted protein was mixed in a 1:1 ratio with Laemmeli's buffer and then loaded onto a 12% sodium dodecyl sulfate-polyacrylamide gel electrophoresis (SDS-PAGE) gel. The gel was run for 90 min at 120 V, and the protein bands on the gel were transferred onto a PVDF membrane. The transferred protein bands on the membrane were then blocked with 3% milk in PBS buffer containing Tween-20 (PBST) for 1 h and incubated overnight at 4°C with 1:1,000 dilution of the primary mouse antibody from Bcl-2 or GADPH in milk. The next day, the milk was decanted and the membrane washed twice with PBST buffer and then incubated with 1:10000 dilution of the secondary anti-mouse goat radish peroxidase (HRP)-conjugated antibody in PBST for 1 h at room temperature. After washing, the ECL reagent was added, which was reacted by the HRP enzyme to give a chemiluminescent band. The chemiluminescent bands were visualized using a Kodak X-ray film.

Evaluation of apoptotic Induction by flow cytometry after various nanoplexes delivery

To assess the apoptotic induction of hybrid nanoparticles under the N/P ratio of 25:1, HEK293 cells were seeded into 6-well plates (1×10^5/well) and incubated for 24 h. The cells were reacted with the above-mentioned formulations (with Bcl-2 siRNA). Lipofectamine was used as the positive control. After 48 h of incubation, the cells were collected and the apoptotic cells were detected by flow cytometry (BD Biosciences) using the annexin V-FITC/propidium iodide (PI) apoptosis detection kit (Invitrogen), according to the standard protocol provided by the suppliers. The results were analyzed using WinMDI 2.9 software.

Results and discussion

Biosafety evaluation of the co-caged delivery vector

The TV was prepared according to our previously reported protocol, [28] in which the detailed characterization and quantum yield were examined and estimated, respectively. In brief, the TV comprised the G_4NH_2 with caging an Au_8-dominating cluster, possessing a strong photoluminescence from the emission maximum appeared approximately 460 nm. Then, the G_4NH_2 was examined for its cytotoxicity before and after being caged with gold-nanoclusters. As expected, severe cell death was observed in the G_4NH_2 alone (Fig. 2A, column 1). Contrary to our expectations, no dosage-dependent cytotoxicity was observed from the TV (Fig. 2A, column 2). In addition to cytotoxicity studies, the immunological response of cells upon exposure to the TV and MTV was also investigated. Dendritic cells (DCs), which play a critical role in initiating immune responses,[31] can be used

to evaluate the immunotoxicity[32] of the TV and MTV. First, we determined the cytotoxicity of the TV and MTV on mouse bone-marrow-derived DCs. The results were consistent, as we found no significant differences between TV and MTV in ESI Fig. S1.† Second, we assessed whether DCs were activated upon treatment with the TV and MTV. In contrast to lipopolysaccharide (LPS) stimulation, neither the TV nor MTV induced the production of cytokine tumor necrosis factor-α (TNF-α) by DCs, suggesting no DC activation by the TV or MTV (Fig. 2B, the left column). Furthermore, the TV and MTV did not promote DC maturation at all, because the expression levels of major histocompatibility complex (MHC) class II (the middle column) and costimulatory molecule CD86 were not changed (Fig. 2B, right column). Collectively, we confirm that the TV and MTV are safe materials that do not provoke immunotoxicity.

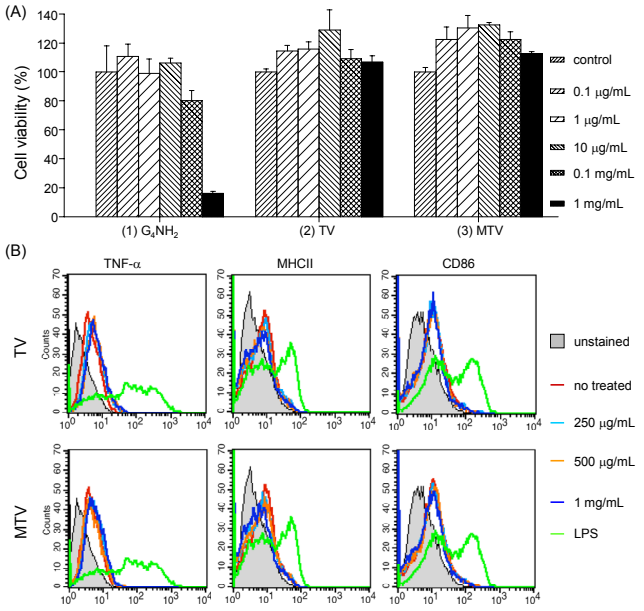

Fig. 2 (A) Cytotoxicity assay for A549 and (B) the impact of siRNA vehicle on immune response. DCs were treated with TV or MTV for 6 h (for TNF-α) or 24 h (for MHC-II and CD86). The expression level of TNF-α, MHC class II and CD86 were determined by flow cytometry. All data were gated on $CD11c^+$ cells.

Physicochemical properties of TV and MTV

Such the significant detoxification may be speculated from the deactivation of outward 1^o-amines, resulting in minimizing the interaction between G_4NH_2 and cell membranes during transfection. Basically, two plausible pathways, such as oxidization and backfolding of 1^o-amines, might be involved in the deactivation. Apparently, no significant amine oxides, such as nitrate and nitrite, from G_4NH_2 can be found in the reaction solution during $HAuCl_4$ reduction in ESI Fig. S2†, indicating that the possible oxidization of 1^o-amines can be ruled out. Alternatively, it is significant because the 1^o-amines of the intact dendrimers are known to easily move out (i.e., branch) and in (i.e., core) of the dendrimer cavity.[33, 34] The backfolding phenomenon of the 1^o-amine groups from branch to the core may induce a strong interaction between the gold surface and the amine groups, which has been studied from amine-capped gold nanoparticles.[35] With the irreversible backfolding, the 1^o-amines of the TV can possibly reduce nucleophilicity to annihilate the intrinsic cytotoxicity. To validate this hypothesis, NMR spectroscopy was used to examine the differences in dendrimer structures before and after caging gold-nanocluster dendrimers. Analysis of the ^1H NMR spectra (ESI Fig. S3†), a specific peak 2.83 ppm arises from overlapping signals the 1^o-amine and 3^o-amine methylenes of the G_4NH_2. The overlapping peak can be split into two peaks at approximately 2.85 and 3.17 ppm after the TV (i.e., G_4NH_2 caging the gold-nanocluster). Such a pronounced peak appearing at the downfield region of NMR spectrum may be affected by the de-shielding effect of gold-nanoclusters. However, this observation cannot fully explain the backfolding of 1^o-amines. To further verify the backfolding phenomenon, a ninhydrin test was used to estimate the 1^o-amine number.[36] As expected, Fig. 3A shows that the absorption wavelength at approximately 560 nm dramatically decreases from the TV, compared with that from G_4NH_2 alone. The percentage of residual 1^o-amines from the TV decreased to approximately 33% of the parent G_4NH_2 after the backfolding; that is, estimating at roughly 20 numbers per G_4NH_2 (the original number is 64 per G_4NH_2). To further examine the dimension of TV, Fig. 3B shows that the entire size is smaller than that of G_4NH_2 without caging the gold-nanocluster. Interestingly, Figure S4 shows a uniform dimension from various dendrimers with smaller and larger generations after caging gold-nanoclusters. We speculated that the size contraction may involve a specific interaction between the dendrimer backbone and gold nanocluster,[37] and then induce the irreversible backfolding of 1^o-amine for the detoxification of dendrimers.

Such the detoxification of G_4NH_2 by caging gold-nanoclusters, however, the values of the zeta potential dramatically decreased from +62.3 mV of the parent G_4NH_2 to +2.8 mV for the TV. This charge neutralization of the TV would affect to associate with the negative charge of siRNA. Thus, the residual 1^o-amines and 3^o-amines of the TV were forced to partially cage methyl-motifs to form the MTV for enhancing siRNA association. Since the 4^o-positive charges of ammonium ions from MTV can strongly associate with the negative siRNA for complex through an electrostatic interaction. Neither noticeable cytotoxicity (Fig. 2A, column 3) nor size change (Fig. 3B, land 6) can be observed from the MTV as well as those of TV. Besides the photoluminescence of the TV, the MTV can exhibit a blue photoluminescence, and the quantum efficiency is slightly stronger than the TV. The percentage of methyl-motifs from 1^o- and 3^o-amines was estimated to be approximately 19% and 21%, respectively. Detailed calculations are listed in ESI Fig. S5† and Table S1†.

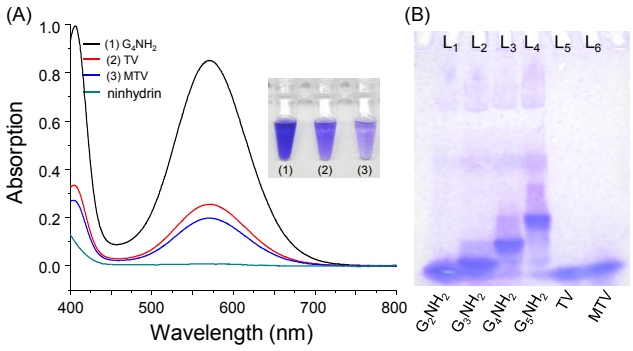

Fig. 3 (A) 1^o-amine number and (B) size of TV and MTV were examined.

Cellular uptake, endosomal escape and cytosolic access

Endocytosis is considered to be the dominant uptake mechanism of dendrimers.[38] Therefore, the dendrimer-based siRNA delivery vehicle's (i.e., TV and MTV) cellular uptake would occur through endocytosis and then coupled with endosomal escape to accelerate siRNA release from the endosome into the cytoplasm for mRNA knockdown. Therefore, the efficiency of endosomal escape should be evaluated prior to studying siRNA transfection. Fig. 4A and B show that the TV and MTV can be taken up by cells, respectively. Using time-course tracking, we found that the MTV can be rapidly internalized by cells compared to the TV, by monitoring the MTV and TV signals after incubation for up to 1.5 h and 48 h, respectively. Presumably, the uptake efficiency may be correlated with the methyl-motifs to increase charges,[39] with a higher charge (+12.6 mV at pH 7.4) being measured from the MTV. Additionally, the fluorescence signal of the TV and MTV can be co-localized with LysoTracker Red (a fluorescent anisotropic probe for cells), demonstrating that our materials were indeed trapped in the endosome and lysosome. Then, a significant signal from the MTV was observed in the cytoplasm after the 48 h-incubation period, indicating that the MTV can escape from the endosome. In contrast, the escape was not observed for the TV at the same time-course. To further estimate the difference of fluorescence signals, the colocalization coefficient (Fig. 4C) and the escape ratios (Fig. 4D) were plotted as a function of time, respectively. Comparatively, only the colocalization coefficient from MTV can gradually decrease accompanying by the increase of escape ratios, indicating that the escape efficiency of MTV was indeed higher than that of TV. This result implies that the MTV may act as a more efficient proton-sponger than the TV. Additionally, this improvement may be explained by the greater intracellular uptake from the MTV than from the TV. This phenomenon can be observed from the disappearance of the lysotracker signal after MTV internalization up to 6 h. Once the basicity of the excess MTV neutralizes the pH of the endosome/lysosome, it results in the inefficient staining from Lysotracker. As expected, the gradual disappearance of the LysoTracker Red signal was observed only in the MTV, indicating that the pH value of these acidic organelles increased significantly in the presence of the MTV, as shown in the time-course pictures. The buffer capacity of the MTV was also found to be slightly higher than that of the TV (the calculation is listed in ESI Table S1†), which might directly cause a more efficient proton-sponge effect and cytosolic access than the TV does. After that, we attempted to examine the intracellular trafficking and distribution of TV/siRNA and MTV/siRNA complexes, respectively. As expected, such the higher siRNA signals (Fig. 5, red colour) can be observed from the MTV/siRNA than those of TV/siRNA, reconfirming that the cytosolic access of MTV was indeed stronger than that of TV. To this end, we would demonstrate the protein induction of siRNA release by flow cytomentry and Western blot in the following experiments.

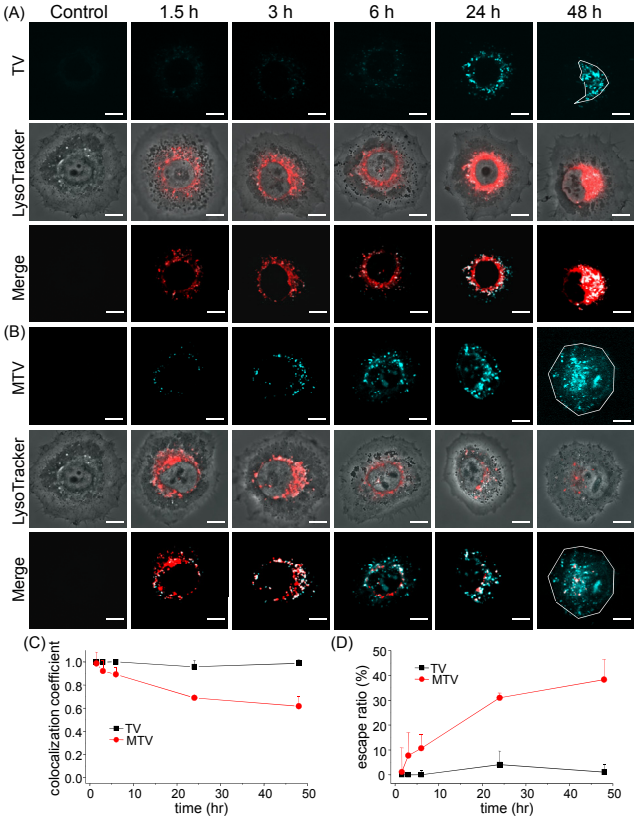

Fig. 4 The intracellular uptake difference between (A) TV and (B) MTV was compared. Confocal fluorescence images of photoluminescent dendrimers in H460 cells at different incubation times (between 1.5h and 48h). H460 cells were co-incubated with Lysotracker (red color) and either TV (blue color) or MTV (blue color). The colocalization of nanoclusters and endosomal/lysosomal compartments were depicted in white color. (C) The colocalization coefficient, and (D) the escape ratios of from TV (block line) and MTV (red line) versus time are calculated. Note that the escape ratios were quantified the fluorescence intensity of TV and MTV after subtracting image background from the co-localization intensity by the metaMorph imaging analysis software. Scale bar 10 μm.

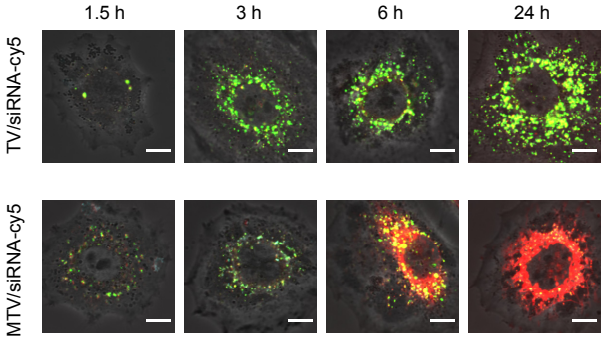

Fig. 5 The intracellular trafficking and distribution difference between (A) TV/siRNA and (B) MTV/siRNA was compared. Note that the cy5-labeled and scramble siRNA was used in the study. Red, green and blue colors represent siRNA-cy5, lysotracker and TV/MTV, respectively. Scale bar 10 μm.

To study the stability of nanoplexes in serum

To investigate whether the TV and MTV can demonstrate significant efficacy in siRNA delivery, or whether the transfection efficiency indeed correlates with the performance of cytosolic access, the TV and MTV were associated with siRNA at various ratios (mol/mol) of amine/phosphate (N/P) to form two types of complexes: TV/siRNA and MTV/siRNA. To further analyze siRNA condensation efficiency, various N/P ratios forming TV/siRNA (ESI Fig. S6A†, lanes 2-5) and MTV/siRNA

(ESI Fig. S6B†, lanes 2-5) were stained with ethidium bromide (EB) after running agarose gel electrophoresis. The EB signal can dramatically decrease accompanied by the MTV/siRNA with an N/P ratio ranging from 25 to 100 compared to those of the TV/siRNA. The disappearance of the EB signal indicates that the condensation efficiency of the MTV/siRNA was higher than that of the TV/siRNA; EB can only insert into free siRNA or loose complex to emit a red fluorescence. The condensation efficiency can be estimated as ranging from 20 to 45% (right panel, black circle) and higher than 80% (right panel, black square) for TV/siRNA and MTV/siRNA, respectively. Subsequently, the siRNA release profiles (ESI Fig. S6A† and B†, lanes 7-10) of these complexes were further studied by treatment with SDS after RNase digestion. Despite the fact that the condensation efficiency of the MTV/siRNA complex was higher than that of the TV/siRNA complex, a stronger EB signal can still be observed from the releasing profiles of the MTV/siRNA (ESI Fig. S6B†, lanes 7-10) rather than from those of the TV/siRNA (ESI Fig. S6A†, lanes 7-10). Apparently, the quantification of siRNA shows almost all siRNA to be released from TV vehicle (right panel, gray circle) rather than from MTV (right panel, gray square), suggesting that the MTV/siRNA complex might more stable than the TV/siRNA complex. These results indicate the structure of the MTV/siRNA complex to be more compact than that of the TV/siRNA complex. TEM images with negative staining (Fig. S7) demonstrated the structural differences between these complexes. The contrast image with black and white can be observed from the TV/siRNA and the MTV/siRNA, respectively, indicating a denser complex from the MTV than the TV. Such the compact complex derived from MTV/siRNA would be verified the stability in serum, the result showing in Fig. 6. It is noteworthily that no significant EB signals can be observed in medium containing 10% or 30% serum (Fig. 6A) as well as no concerns from degradation since the siRNA still can be released by SDS replacement (Fig. 6B). The results indicated that the siRNA can be well-protected by MTV to prevent serum digestion.

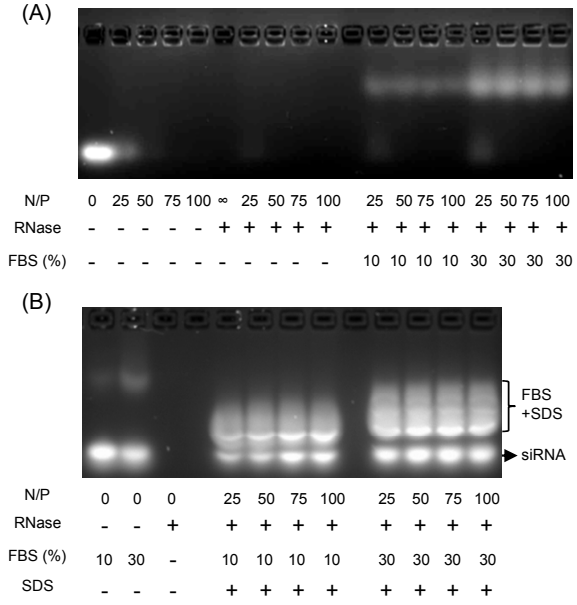

Fig. 6 (A) The stability of MTV/siRNA complexes in the presence of serum was evaluated. (B) To demonstrate the well-protected siRNA by the MTV vehicle can be measured after the SDS replacement. Note that the smear bands above the siRNA signals were the mixtures of SDS and serum.

Induction of apoptosis by siRNA silencing

To study whether the MTV with efficient siRNA protection and cytosolic access can directly affect the silencing efficiency, the MTV was associated with Bcl-2 siRNA to form complexes. To test the silencing performance, the HEK 293 cells were used to perform the mRNA knockdown of Bcl-2, a well-known key inhibitor of apoptosis induced in mammalian cells,[40] by using Bcl-2 siRNA. Fig. 7A shows that the viability of cells treated with the MTV/Bcl-2 siRNA complex was found to decrease approximately to 75 %, which was almost the same as the treatment with siRNA commercial transfection agent (lipofectamine decreased to approximately 75 %). The quantification of silencing efficiency displayed in the Fig. 7B, in which the apoptotic effect in each sample was assessed by gating cell populations from early (top right quadrant) and lately apoptotic stages (bottom right quadrant). Apparently, the percentage of apoptosis induction is 25% from the MTV/siRNA complex as well as that of Lipofectamine complex. This result demonstrates that siRNA transfection can indeed be improved by using an excellent endosome-escape vector (i.e., MTV) to cytosolic access. Such efficient silencing can be confirmed by the Western-Blot result (Fig. 7C) as well. As expected, a significant down-regulation in Bcl-2 can be observed from the MTV (the right column) compared to other groups (siRNA-alone, MTV-alone, MTV/scramble siRNA), and the efficiency was similar to that of Lipofectamine. These results indicate that the MTV/Bcl-2 siRNA complex can efficiently induce cell apoptosis.

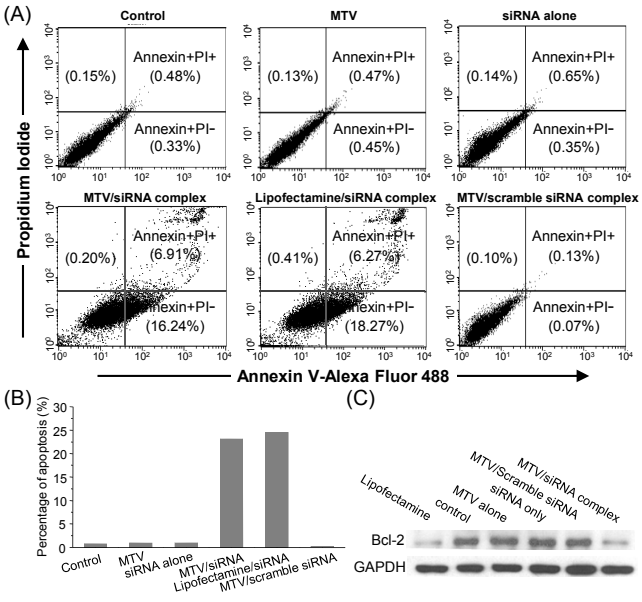

Fig. 7 (A) Population of cell apoptosis analyzed by flow cytometry under various treatments for 72 h, the HEK 293 cells after treating four conditions: control, siRNA-alone, MTV/siRNA, lipofectamine/siRNA and MTV/scramble siRNA, respectively. (B) To quantify the efficiency of apoptosis induction from the multiple sets of nanoplexes. Note that the percentages of apoptosis induction from various nanoplexes were calculated from the total value within the top and bottom right quadrant per each profile. (C) The silencing efficiency of Bcl-2 was analyzed by Western blot.

Conclusion

In summary, we developed a simple and novel strategy based on co-caging gold-nanoclusters and methyl-motifs that leads to detoxification of dendrimers and allow cystolic access for siRNA Transfection. By embedding tiny gold-nanoclusters, the structures of dendrimer become compact that induce an irreversible backfolding of the outer primary amines from the branch to the core, which dramatically reduces the toxicity of the dendrimers, enhancing their safety. The co-presence of methyl-motifs can enhance cytosolic access of dendrimers to deliver siRNA for mRNA knockdown. This finding provides a novel perspective to facilitate various cationic polymers for detoxification in biological applications through a co-caging strategy without further chemical modifications.

Acknowledgements

The authors are grateful to the National Health Research Institutes of Taiwan (NHRI-NM-102-PP-10) and the Ministry of Science and Technology of Taiwan (NSC-100-2113-M-400-001-MY3) for providing financial support for this research. A part of this work was supported by grant 100R311001 from the College of Medicine, National Taiwan University (to CLC). The authors would also like to thank Y-L Yu and T-H Wu (NHRI) for providing technical support.

Notes and references

[a] *Institute of Biomedical Engineering and Nanomedicine, National Health Research Institutes, No. 35 Keyan Road Zhunan, Miaoli County, 35053 (Taiwan)*
[b] *Graduate Institute of Immunology, College of Medicine, National Taiwan University, 5F, No 1, Sec 1, Jen-Ai Rd Taipei, 10051 (Taiwan).*

† Electronic Supplementary Information (ESI) available: [details of any supplementary information available should be included here]. See DOI: 10.1039/b000000x/

1 J. H. Zhou, J. Y. Wu, N. Hafdi, J. P. Behr, P. Erbacher and L. Peng, *Chem. Commun.*, 2006**,** 2362-2364.
2 M. A. Mintzer and E. E. Simanek, *Chem. Rev.*, 2009, **109,** 259-302.
3 A. L. Becker, A. P. R. Johnston and F. Caruso, *Small*, 2010, **6,** 1836-1852.
4 T. Froehlich and E. Wagner, *Soft Matter*, 2010, **6,** 226-234.
5 P. Kesharwani, V. Gajbhiye and N. K. Jain, *Biomaterials*, 2012, **33,** 7138-7150.
6 S. K. Samal, M. Dash, S. Van Vlierberghe, D. L. Kaplan, E. Chiellini, C. van Blitterswijk, L. Moroni and P. Dubruel, *Chem. Soc. Rev.*, 2012, **41,** 7147-7194.
7 P. R. Leroueil, S. Y. Hong, A. Mecke, J. R. Baker, B. G. Orr and M. M. B. Holl, *Acc. Chem. Res.*, 2007, **40,** 335-342.
8 N. D. Sonawane, F. C. Szoka and A. S. Verkman, *J. Biol. Chem.*, 2003, **278,** 44826-44831.
9 M. A. Mintzer and M. W. Grinstaff, *Chem. Soc. Rev.*, 2011, **40,** 173-190.
10 N. Malik, R. Wiwattanapatapee, R. Klopsch, K. Lorenz, H. Frey, J. W. Weener, E. W. Meijer, W. Paulus and R. Duncan, *J. Controlled Release*, 2000, **65,** 133-148.
11 Z.-Y. Zhang and B. D. Smith, *Bioconjug. Chem.*, 2000, **11,** 805-814.
12 A. Mecke, I. J. Majoros, A. K. Patri, J. R. Baker, M. M. B. Holl and B. G. Orr, *Langmuir*, 2005, **21,** 10348-10354.
13 K. Jain, P. Kesharwani, U. Gupta and N. K. Jain, *Int. J. Pharm.*, 2010, **394,** 122-142.
14 I. J. Majoros, B. Keszler, S. Woehler, T. Bull and J. R. Baker, *Macromolecules*, 2003, **36,** 5526-5529.
15 K. Kono, H. Akiyama, T. Takahashi, T. Takagishi and A. Harada, *Bioconjug. Chem.*, 2005, **16,** 208-214.
16 R. B. Kolhatkar, K. M. Kitchens, P. W. Swaan and H. Ghandehari, *Bioconjug. Chem.*, 2007, **18,** 2054-2060.
17 M. L. Patil, M. Zhang, S. Betigeri, O. Taratula, H. He and T. Minko, *Bioconjug. Chem.*, 2008, **19,** 1396-1403.
18 A. Saovapakhiran, A. D'Emanuele, D. Attwood and J. Penny, *Bioconjug. Chem.*, 2009, **20,** 693-701.
19 H. Lee and R. G. Larson, *J. Phys. Chem. C*, 2011, **115,** 5316-5322.
20 L. Albertazzi, L. Gherardini, M. Brondi, S. S. Sato, A. Bifone, T. Pizzorusso, G. M. Ratto and G. Bardi, *Mol. Pharm.*, 2013, **10,** 249-260.
21 L. G. Wang, Z. Wang, G. L. Ma, W. F. Lin and S. F. Chen, *Langmuir*, 2013, **29,** 8914-8921.
22 H. Kobayashi, C. C. Wu, M. K. Kim, C. H. Paik, J. A. Carrasquillo and M. W. Brechbiel, *Bioconjug. Chem.*, 1999, **10,** 103-111.
23 L. M. Kaminskas, B. J. Boyd and C. J. H. Porter, *Nanomedicine*, 2011, **6,** 1063-1084.
24 S. Sadekar, A. Ray, M. Janat-Amsbury, C. M. Peterson and H. Ghandehari, *Biomacromolecules*, 2011, **12,** 88-96.
25 X. F. Lu, Y. Liu, X. J. Kong, P. E. Lobie, C. Y. Chen and T. Zhu, *Small*, 2013, **9,** 1654-1671.
26 K. Fant, E. K. Eshjorner, A. Jenkins, M. C. Grossel, P. Lincoln and B. Norden, *Mol. Pharm.*, 2010, **7,** 1734-1746.
27 C. L. Waite, S. M. Sparks, K. E. Uhrich and C. M. Roth, *BMC Biotechnology*, 2009, **9**.
28 Y. C. Jao, M. K. Chen and S. Y. Lin, *Chem. Commun.*, 2010, **46,** 2626-2628.
29 Y. L. Yu, I. H. Chen, K. Y. Shen, R. Y. Huang, W. R. Wang, C. J. Chou, T. T. Chang and C. L. Chu, *Eur. J. Immunol.*, 2009, **39,** 2482-2491.
30 R. Y. Huang, Y. L. Yu, W. C. Cheng, C. N. OuYang, E. Fu and C. L. Chu, *J. Immunol.*, 2010, **184,** 6815-6821.
31 R. M. Steinman, *Annu. Rev. Immunol.*, 2012, **30,** 1-22.
32 C. L. Villiers, H. Freitas, R. Couderc, M. B. Villiers and P. N. Marche, *J. Nanopart. Res.*, 2010, **12,** 55-60.
33 R. L. Lescanec and M. Muthukumar, *Macromolecules*, 1990, **23,** 2280-2288.
34 J. Haensler and F. C. Szoka, *Bioconjug. Chem.*, 1993, **4,** 372-379.
35 P. R. Selvakannan, S. Mandal, S. Phadtare, R. Pasricha and M. Sastry, *Langmuir*, 2003, **19,** 3545-3549.
36 E. Kaiser, Colescot.Rl, Bossinge.Cd and P. I. Cook, *Anal. Biochem.*, 1970, **34,** 595-598.
37 K. Torigoe, A. Suzuki and K. Esumi, *J. Colloid Interface Sci.*, 2001, **241,** 346-356.
38 K. M. Kitchens, A. B. Foraker, R. B. Kolhatkar, P. W. Swaan and H. Ghandehari, *Pharm. Res.*, 2007, **24,** 2138-2145.
39 M. L. Patil, M. Zhang, O. Taratula, O. B. Garbuzenko, H. He and T. Minko, *Biomacromolecules*, 2009, **10,** 258-266.
40 M. Jiang and J. Milner, *Genes & development*, 2003, **17,** 832-837.